Force Ripple and Cogging Force Minimisation Criteria of Single-Sided Consequent-Pole Linear Vernier Hybrid Machines

C.D. Botha, M.J. Kamper, R.-J. Wang, and A.J. Sorgdrager

***Abstract*—In this paper, the force ripple and cogging force minimisation of single-sided consequent-pole linear vernier hybrid machines is investigated through the use of the Taguchi method. The study focuses on obtaining robust designs that minimise the force ripple and cogging force through optimal tapering of the translator teeth, the soft ferromagnetic consequent poles and the permanent magnets. It is found that by minimising the force ripple a better overall design solution can be found, effectively minimising both the force ripple and cogging force, while limiting the reduction in average thrust force. The percentage contribution of each parameter is analysed, from which a trend is identified and broad criteria for the taper ratios are defined.**

***Index Terms*—Consequent pole, design optimisation, force ripple, linear vernier hybrid machines, Taguchi method**

I. Introduction

The use of linear electric machines (LEMs) in direct-drive applications is an attractive option, as they eliminate the need for intermediate rotary-to-linear conversion systems, reducing the overall system cost and improving the reliability [1]. For low-speed, direct-drive applications, the conventional linear permanent magnet (PM) machine is relatively bulky, as the space required to house multiple pole pairs' armature windings is quite large [1], [2], thus the system cost is high. As an alternative, the linear vernier PM machines [1], [3], [4] and the linear vernier hybrid machines (LVHMs) [2], [5] have been proposed for low-speed applications.

The working of both machine types is based on the magnetic gearing effect, where the flux of multiple magnets links with a single armature pole pair. These machines thus have a very high force density. However, the high number of PMs are also the cause of a large leakage flux, which results in a low operating power factor.

In this paper, single-sided consequent-pole (CP) LVHMs are investigated. With the consequent-pole configuration, about 50 % of the PMs of a LVHM are replaced with soft ferromagnetic poles, which reduce the amount of PM material used without negatively affecting the machine performance [6], and in some cases even leads to improved machine performance [5]. A previous study shows that the teeth tapering of the consequent pole can improve the thrust force quality [2]. However, this technique alone may not be sufficient to lower the cogging force and/or thrust force ripple to a desired level.

To investigate the separate and combined effects of tapering the CP teeth, PMs and translator teeth have on force ripple and cogging force, the Taguchi method is used in this study in an attempt to find a solution that effectively minimises both in CP LVHMs.

The paper proceeds as follows: Section II describes the machine configurations and the operating principle of the CP LVHMs. Section III explains the design optimisation framework using the Taguchi method. In Section IV, the results and comparison of the design optimisation are presented, and the relevant conclusions are drawn in Section V.

II. Machine Topologies and Operating Principles of the CP LVHM

A. Configurations

The different CP LVHM configurations are shown in Fig. 1, with the specifications of each being given in Table I. The investigation is done on a 500 N thrust force level, with each machine designed to provide 500 N at an efficiency of 90 % or above using only q-axis current. In order to improve the quality of the thrust force and reduce the cogging force, tapering schemes including the consequent poles, PMs as well as the translator teeth are considered. The different taper ratios, defined by (1) to (3), are illustrated in Fig. 2, where w_{PM} is the magnet width, $k_{c_{N/S}}$ is the CP taper ratio, and with the N/S subscript indicating whether the ferromagnet pole is adjacent to a north or south pole magnet, k_m is the magnet tapering ratio and k_t is the translator tooth tapering ratio.

B. Operation Principles

The CP LVHM operates on the principle of magnetic flux modulation, converting a slow rate of change in mechanical position to a high rate of change in flux. When a magnet pole pair is aligned with the translator, the coil flux linkage reaches its maximum value. As the magnet pole pair moves a quarter of the translator pole pitch, the coil flux linkage

The research presented in this paper is financially sponsored by the Centre for Renewable and Sustainable Energy Studies (CRSES) in Stellenbosch, South Africa.

C. D. Botha, M. J. Kamper and R-J. Wang are with the Department of Electrical and Electronic Engineering, Stellenbosch University, South Africa (e-mail:17058945@sun.ac.za; kamper@sun.ac.za; rwang@sun.ac.za).

A. J. Sorgdrager is with the Magna Powertrain, St. Valentin, Austria (e-mail:ajsorgdrager@gmail.com)

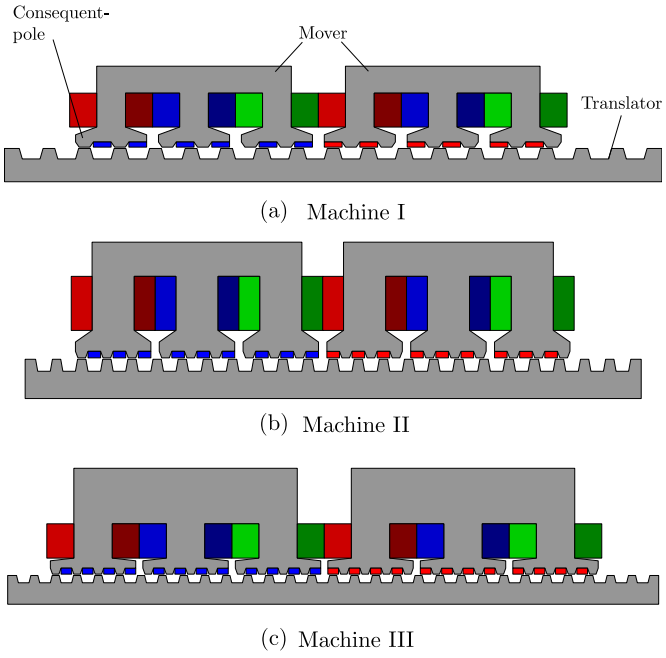

Fig. 1. CP LVHM configurations considered in this study.

TABLE I
CONSEQUENT-POLE MACHINE SPECIFICATIONS

Parameters	Machine I	Machine II	Machine III
Force (N)	500	500	500
Current density (A/mm^2)	3.33	2.3	2.39
Efficiency (%)	90	92.8	92
Force ripple (%)	11.8	10.5	8.9
Cogging force (%)	12.97	4	4.7
PM pole pair/mover tooth	2	3	4
Magnet width (mm)	13	9.2	7.8
Magnet thickness (mm)	3.8	4.8	4.4
Magnet remanence (T)	1.3	1.3	1.3
air gap (mm)	1	1	1

reaches the minimum. Moving one translator pole pitch is equivalent to one full electrical cycle. This produces a rapid change in flux linkage with small mechanical movement.

This flux modulation principle is illustrated in Fig. 3 for a single mover unit with two PM pole pairs per mover tooth, where p_m is the PM pole pairs and p_t is the number of

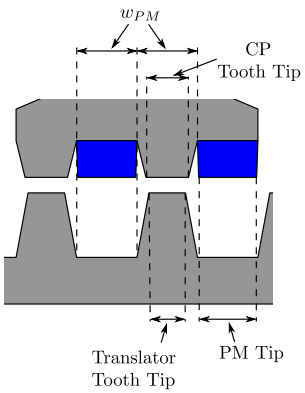

$$k_t = \frac{\text{Translator tooth tip}}{w_{PM}} \quad (1)$$

$$k_{c_{N/S}} = \frac{\text{CP tooth tip}}{w_{PM}} \quad (2)$$

$$k_m = \frac{\text{PM tip}}{w_{PM}} \quad (3)$$

Fig. 2. Different tapering ratios used in this paper.

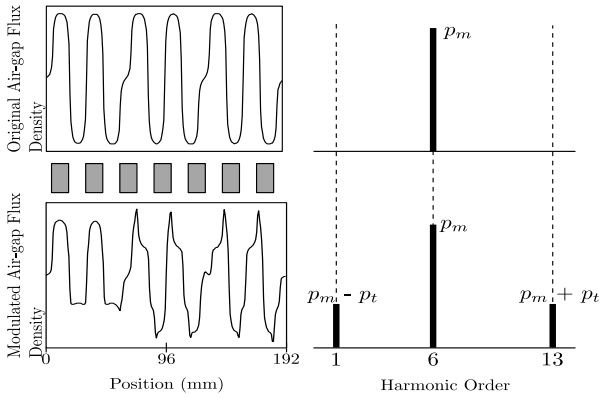

Fig. 3. Flux modulation principle, illustrated for a single mover unit with two PM pole pairs per mover tooth.

active translator teeth. The modulated air gap flux density contains three major components, namely the harmonic term produced by the PM pole pairs and two terms produced due to the modulation by the translator teeth.

The armature winding needs to be designed to have the same pole pairs as one of these two components, generally the lower-order harmonic for LVHMs, to produce useful thrust force.

III. THE TAGUCHI METHOD

The Taguchi method, developed by Dr Genichi Taguchi in the 1940s [7], is an improved design of experiments (DoE) method. It aims to determine an optimal design solution, which is robust and stable, rather than a definite optimum point [8]. The Taguchi method involves the use of special tables known as orthogonal arrays (OAs), wherein the number of trials and parameter values are predefined.

The advantages of the Taguchi method include independence from the initial condition, the ease of determining the subsequent parameter values, reduced parameter complexity, and the insight it provides into the interaction between the parameters [8], [9]. Another important aspect of the Taguchi method is that it allows a sensitivity analysis to be performed using the same design framework. This enables a designer to determine the robustness of the final design when it is subjected to the variations in the optimum parameter values, such as those that manufacturing tolerances are likely to introduce.

Although there are other methods that are used for robust design, such as a Monte Carlo simulation or a Taylor series expansion, the Taguchi method is computationally more efficient and less complex [10].

The use of the Taguchi method for the design of electrical machines has been rather limited, as the method is not well suited for iterative design optimisation. Some recent research has attempted to address these limitations associated with the Taguchi method and has applied the method for single-objective [11], [12] and multi-objective [8], [13] design optimisations on various machine topologies [9]. In [8], the Taguchi-based regression rate (TBRR) approach

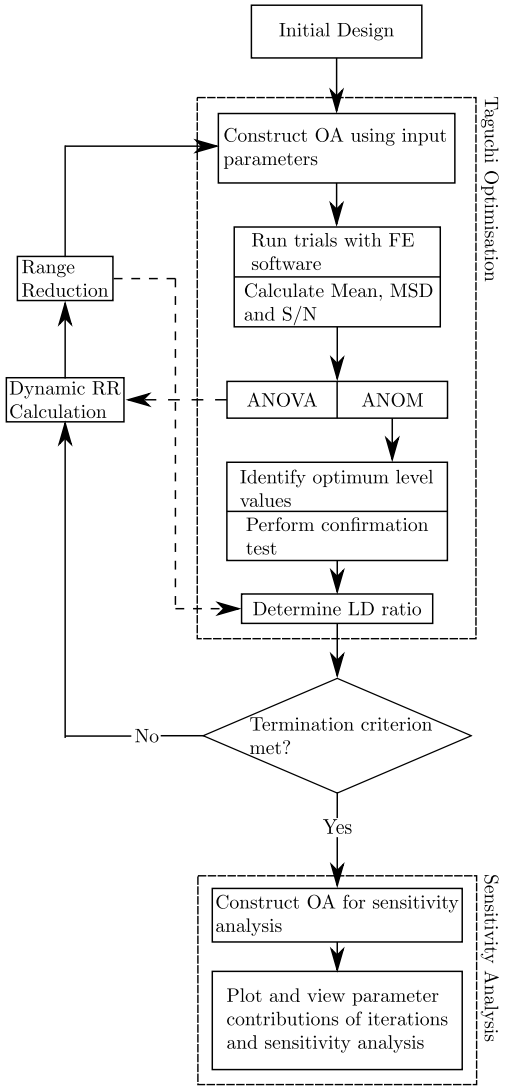

Fig. 4. The Taguchi-based optimisation framework.

was proposed and successfully implemented in the design of electrical machines. In Fig. 4 presents an adaptation of this framework, with each block described in the following subsections.

A. Taguchi Optimisation

The initial design choices form the most important part of the design optimisation. These include investigating different possible orthogonal arrays, deciding on the parameters and their ranges, and determining a fitness function and termination criteria.

A specific OA refers to a certain parameter combination, which consists of a number of levels, i.e. the number of values each parameter has, and the number of parameters. This study uses an L9 (3^4) orthogonal array, similar to the one used in [11], of which an example is given in Table II. This OA has four input parameters, with three levels each, consisting of nine trials.

TABLE II
AN EXAMPLE OF THE L9 OA.

L9	k_{cS}	k_{cN}	k_m	k_t	R_1	R_2	R_3	R_4	Mean	MSD	S/N
T1	L1	L1	L1	L1							
T2	L1	L2	L2	L2							
T3	L1	L3	L3	L3							
T4	L2	L1	L2	L3							
T5	L2	L2	L3	L1							
T6	L2	L3	L1	L2							
T7	L3	L1	L3	L2							
T8	L3	L2	L1	L3							
T9	L3	L3	L2	L1							
				B_r	T	T	M	M			
				t_{PM}	T	M	T	M			

The design can also be exposed to certain "noise" factors through the use of an outer array, which further ensures the robustness of the design.

The input parameters are the taper ratios described in the previous section, while the noise factors are the PM remanence, B_r, and the magnet thickness, t_{PM}. Each iteration of the TBRR method thus consists of nine main candidate trials, requiring four noise conditions and resulting in 36 simulations.

As the simulations are predefined for each iteration, the use of parallel computation may be considered and, in doing so, reduces the overall optimisation time.

After the parameters are chosen and the value ranges are determined, the OA can be initialised. On the first iteration, the minimum and maximum values of each parameter are assigned to L1 and L3, respectively, with L2 being a mid-range value. The initial level difference (LD) is then calculated as

$$\mathrm{LD}_{n_1} = \frac{\mathrm{L}_{n_{max}} - \mathrm{L}_{n_{min}}}{\text{number of levels} + 1}, \tag{4}$$

where $\mathrm{L}_{n_{min}}$ and $\mathrm{L}_{n_{max}}$ are the minimum and maximum value of the n^{th} parameter, respectively. The LD is used to determine the parameter range of the subsequent iteration, as well as the termination criterion. As an outer noise array is used, a mean, a mean square deviation (MSD) and a signal-to-noise (S/N) are calculated for each trial.

The MSD is calculated in accordance with *the smaller-is-better* characteristic and is given as follows:

$$\mathrm{MSD} = \frac{\mathrm{R}_1^2 + \mathrm{R}_2^2 + \mathrm{R}_3^2 + \mathrm{R}_4^2}{4}, \tag{5}$$

where $\mathrm{R}_1 \rightarrow \mathrm{R}_4$ are the outputs of a given trial. The S/N is calculated based on the MSD, and is given by

$$\mathrm{S/N} = -10\log(\mathrm{MSD}). \tag{6}$$

The results of each iteration are analysed through the analysis of the mean (ANOM) of each trial's S/N. This determines the average effect of each parameter value on the OA's results, and is used to identify the optimum value of each parameter. The optimum candidates' performance is

then confirmed using the same noise conditions as the main OA candidates.

For the next iteration, the new LD for each parameter is calculated by

$$\mathrm{LD}_{n_{i+1}} = \mathrm{RR} \cdot \mathrm{LD}_{n_i}, \tag{7}$$

where RR is the regression rate. While it is possible to use a fixed regression rate, this could have a negative impact on the optimisation, as a larger RR slows the LD convergence, requiring more iterations, and a smaller RR increases the risk of a poor design optimisation [8].

A better option is to use the feedback from the current iteration to determine a dynamic regression rate (RR_{dyn}) for each parameter [8], as follows:

$$\mathrm{RR}_{dyn} = (\mathrm{RR}_{max} - \mathrm{RR}_{min}) \frac{\sigma_n^2}{100} + \mathrm{RR}_{min}, \tag{8}$$

where RR_{max} is 0.95, RR_{min} is 0.5, and σ^2 is the percentage contribution of the n^{th} parameter, calculated from the analysis of variance (ANOVA) of the parameter's S/N ratio. Using this approach, each parameter has its own RR, which is related to its contribution to the current iteration's performance variance. Using the newly determined LD, the subsequent iteration's OA can then be constructed.

The fitness function is defined as the force ripple or the cogging force. As stated in the equation below, the termination criterion is met when the LD ratio is lower than the converged value (CV).

$$\frac{LD_{n_i}}{LD_{n_1}} < CV, \tag{9}$$

with CV usually chosen as 0.01 or 0.001.

B. Sensitivity Analysis

The final step, after an optimum design solution is found, is to perform a sensitivity analysis. This analysis uses the same OA shape as described above. The optimum values for each parameter are placed in L2, with this value then varied by 10 % to determine the L1 and L3 values. A bar plot is then used to display and investigate each parameter's contribution to the results of each iteration and the sensitivity analysis.

IV. Comparison and Analysis of Results

Two separate optimisations are performed for each of Machine I, II and III, with the fitness function being the force ripple and cogging force, respectively. The optimisation results are given as force ripple and cogging force minimisation in Fig. 5, together with the baseline values from Table I.

As no force constraint is included in the implementation of the Taguchi method, all three machines have a slight reduction in average thrust force, as shown in Fig. 5(a). This can be expected, as the force quality optimisation is a fine-tuning process before finalising the design. However, the reductions are all within a range of 4–6 %, with the cogging force optimisation of Machine II having the largest average force reduction of 27 N. Machine III has the smallest reduction in average thrust force of 13 N.

TABLE III
Optimum tapering ratios for each machine

	Machine I		
	Baseline value	Force ripple optimum	Cogging force optimum
k_{c_N}	0.6	0.67	0.74
Δx	0	0.915	1.83
k_{c_S}	0.6	0.73	0.72
Δx	0	1.89	1.77
k_m	1	0.92	0.88
Δx	0	-1.04	-1.57
k_t	0.66	0.63	0.6
Δx	0	-0.39	-0.78
	Machine II		
	Baseline value	Force ripple optimum	Cogging force optimum
k_{c_N}	0.6	0.68	0.66
Δx	0	0.74	0.55
k_{c_S}	0.6	0.73	0.68
Δx	0	1.2	0.74
k_m	1	0.92	0.875
Δx	0	-0.74	-1.16
k_t	0.66	0.6	0.6
Δx	0	-0.55	-0.55
	Machine III		
	Baseline value	Force ripple optimum	Cogging force optimum
k_{c_N}	0.6	0.71	0.7
Δx	0	0.86	0.78
k_{c_S}	0.6	0.73	0.69
Δx	0	1.02	0.71
k_m	1	0.89	0.88
Δx	0	-0.86	-0.94
k_t	0.66	0.6	0.6
Δx	0	-0.48	-0.48

All three machines display a significant reduction in force ripple after the force ripple minimisation, shown in Fig. 5(b), with the optimum ripple values for Machine I, II and III being 6.2 %, 6.1 % and 3.75 %, respectively. The cogging force of each machine is also significantly reduced as a result of the force ripple minimisation, with the cogging force of Machine I reduced to 8.2 %, and both Machine II and III reaching cogging forces below 3 % of the rated thrust force.

The cogging force minimisation of the machines, shown in Fig. 5(c), produces similar reductions, with the optimum cogging force values for Machine I, II and III being 4 %, 3.3 % and 2.1 %, respectively.

It should be noted that, for Machine II, the force ripple minimisation actually results in a lower cogging force than the cogging force minimisation, while for Machine III the two minimisations produce near identical results. This is likely due to the nature of the Taguchi method, as it searches for an optimum solution that is robust, rather than a definitive optimum.

The optimum tapering ratios for each optimisation are given in Table III. Alongside the tapering ratios, a Δx is also given. This is the change, in mm, that occurs in the tip of either the tooth or the PM. A positive value indicates the tooth/PM tip has increased, with a negative value indicating the opposite. A few observations on the tapering ratios can be

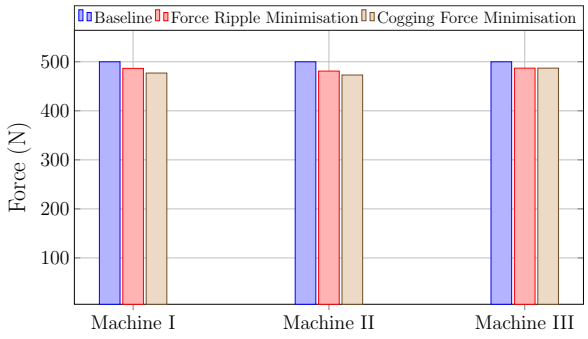

(a) Comparison of average thrust force

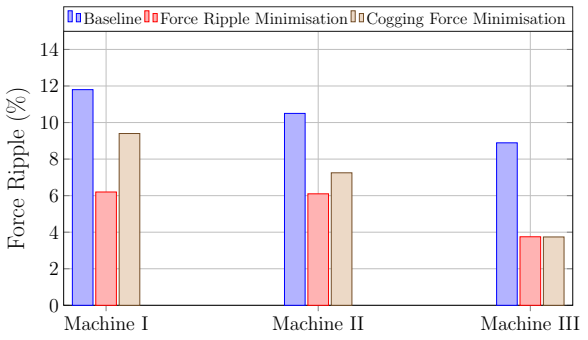

(b) Comparison of force ripple

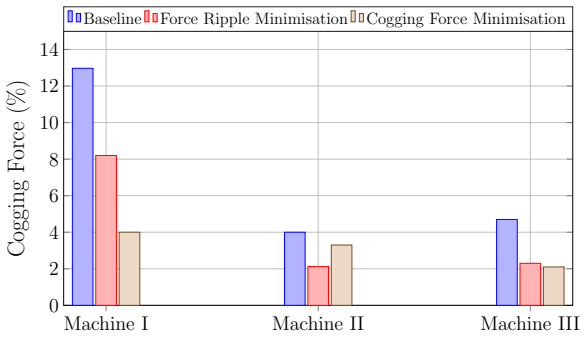

(c) Comparison of cogging force

Fig. 5. Results of the force ripple and cogging force minimisations.

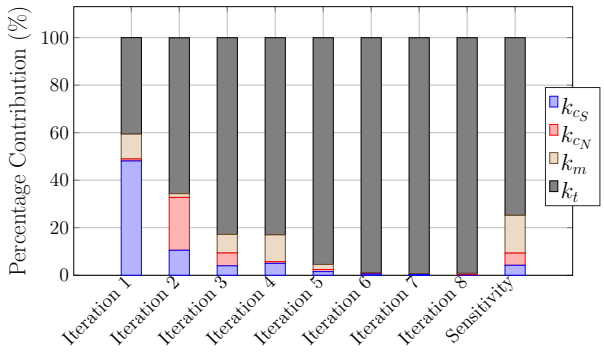

(a) Percentage contribution of each tapering ratio during the force ripple minimisation

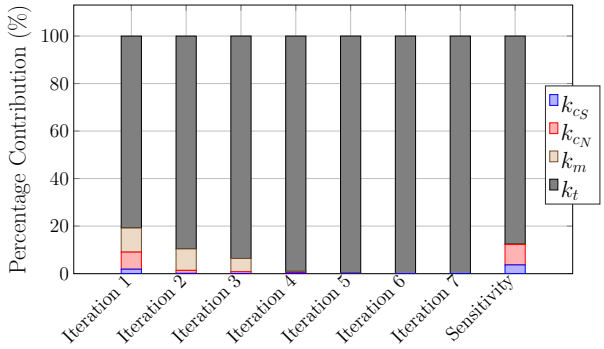

(b) Percentage contribution of each tapering ratio during the cogging force minimisation

Fig. 6. Percentage contribution of each tapering ratio during the trials and the sensitivity analysis for Machine I.

made from these values, such as the identical optimum value of k_t for all three machines in the cogging force optimisation, with the force ripple optimisation also producing the same k_t ratio for Machine II and III.

Similarly, k_{cS} is generally tapered less than k_{cN}, with the only exception being the optimum values for cogging force minimisation in Machine I and III, and the value of k_m converges on 0.9 for all the machine optimisations.

Machine I has the most variance in tapering ratios between the two optimisations, which explains why the performance results of the two optimisations differ so much. The force ripple and cogging force minimisation of Machine III result in very similar tapering ratios, and thus both optimisations produce the same thrust force and force ripple and very similar cogging forces.

To further investigate the effect of each tapering ratio, Figs. 6 – 8 show the effective contributions of each tapering ratio on the force ripple and cogging force of Machine I, II and III, respectively.

The significant effect that k_t has on the cogging force is clear from these graphs, and helps explain why all three machine designs converge on a similar k_t ratio. It is only during the force ripple minimisation of Machine III that k_t does not have an overwhelmingly large effect on the performance outcome. The same pattern is visible for the sensitivity analysis of each machine, with the force ripple of Machine III being the least sensitive to change in the value of k_t. This further confirms the importance of k_t when designing and manufacturing a CP LVHM.

Examining the sensitivity analysis of each optimisation, the optimum force ripple result of Machine III would likely be the most robust of all the designs, as none of the parameters contribute a large amount to the performance variance. The cogging force minimisation of Machines I and III is likely to be the least robust, as a small variation in k_t is likely to lead to a large variation in cogging force. It is interesting to note that the two solutions for Machine III have similar tapering ratios, but the one is less robust than the other.

To illustrate the robustness of the Taguchi optimum design solution, the signal-to-noise (S/N) ratio of each trial from the sensitivity analysis of the baseline and optimised machines is shown in Fig. 9. The variance around the average S/N ratio for the three optimised machines is less than the baseline

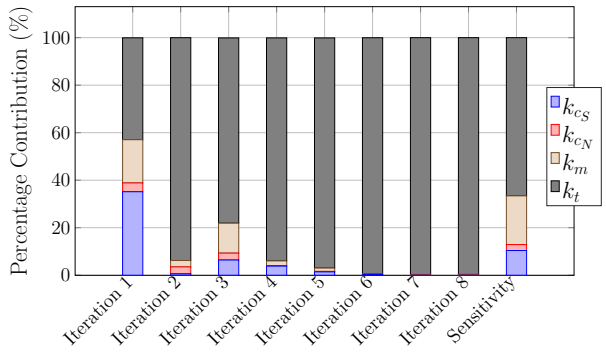

(a) Percentage contribution of each tapering ratio during the force ripple minimisation

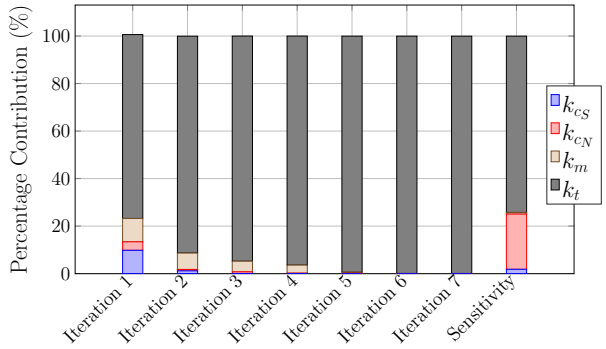

(b) Percentage contribution of each tapering ratio during the cogging force minimisation

Fig. 7. Percentage contribution of each tapering ratio during the trials and the sensitivity analysis for Machine II.

machines. This indicates that the final design solutions are more robust, with Machine II being the most robust, as it has the lowest variance.

A. *Confirmation Tests*

As a further confirmation to the effectiveness of the Taguchi method-based ripple/cogging force minimisation, three additional machines, called Machine I B, II B and III B, are investigated. These machines are also designed to provide 500 N thrust force at an efficiency of 90 % or above; however, the force ripple and cogging forces of these machines are much worse than the previous baseline machines.

The results of these optimisations are shown in Table IV. A similar trend as shown in Fig. 5 is evident, i.e., a more optimum overall solution can be found by minimising force ripple instead of cogging force.

As an example of the results, the optimum tapering ratios of the force ripple minimisation for Machine III B are 0.65, 0.7, 0.88 and 0.63, for k_{c_N}, k_{c_S}, k_m and k_t, respectively. These are very similar to the values given in Table III.

While the force ripple and cogging force of each machine is lowered, the final design solutions do not achieve the same level of low force ripple and cogging force as the previous three machines. This highlights a limitation of ripple/cogging force minimisation through the use of the four tapering ratios. The initial force ripple and cogging force values of

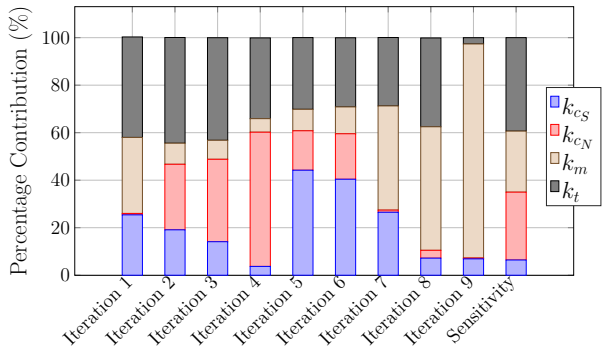

(a) Percentage contribution of each tapering ratio during the force ripple minimisation

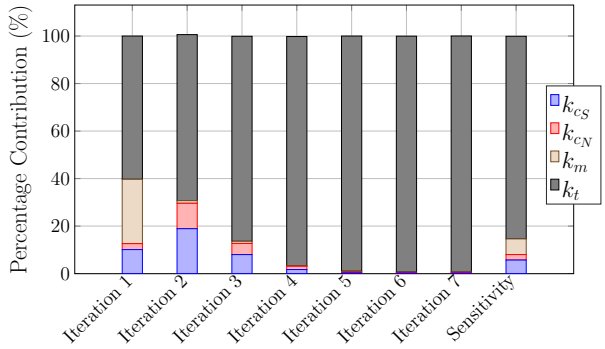

(b) Percentage contribution of each tapering ratio during the cogging force minimisation

Fig. 8. Percentage contribution of each tapering ratio during the trials and the sensitivity analysis for Machine III.

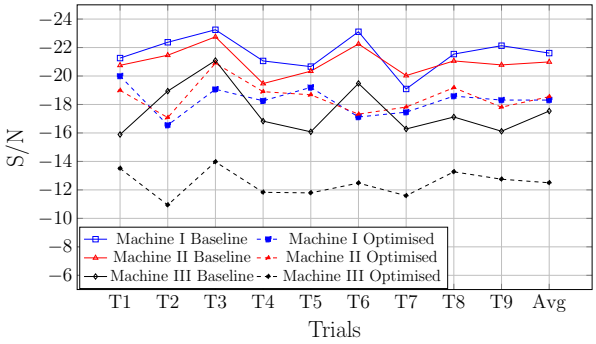

Fig. 9. Comparison of the S/N ratios of the sensitivity analysis for the baseline and Taguchi force ripple optimum of Machine I, II and III.

the machine are thus also important when implementing the proposed method.

V. Conclusion

In this paper, the Taguchi method is used to minimise the force ripple and cogging force of three 500 N CP LVHMs. Using a simple L9 OA with four tapering ratios as the input parameters, the force ripple and cogging force can be reduced significantly. The use of the Taguchi method also allows for investigating the effect and mutual interaction of the tapering ratios on the machine performance, and produces a more robust design with a slight reduction in average thrust force.

TABLE IV
RESULTS FROM THE TAGUCHI METHOD OPTIMISATIONS OF THE ADDITIONAL MACHINES

	Machine I B		
	Baseline value	Force ripple optimum	Cogging force optimum
Force (N)	500	480	479
Force Ripple (%)	30	19.5	28
Cogging Force (%)	19.7	12.3	6.3
	Machine II B		
	Baseline value	Force ripple optimum	Cogging force optimum
Force (N)	500	482	471
Force Ripple (%)	17.6	9.2	16.3
Cogging Force (%)	8.3	8.5	4.1
	Machine III B		
	Baseline value	Force ripple optimum	Cogging force optimum
Force (N)	500	480	472
Force Ripple (%)	16.9	10.5	13.5
Cogging Force (%)	12.9	7.9	4.4

The results of the studied cases in this paper show that, by minimising the thrust force ripple, a better overall design solution can be found, as it effectively minimises both the force ripple and cogging force, while not reducing the average thrust force as much as the cogging force minimisation.

The different tapering ratios have a significant effect on the force ripple and cogging force performance of the CP LVHM. The k_t makes the largest contribution during the force ripple and cogging force minimisation, with a larger taper generally resulting in a lower cogging force and force ripple.

Tapering one mover's CP slightly more than the others appears to also help in minimising both the ripple and cogging effect. The taper ratios for the magnets are very similar throughout, indicating that a small taper in the magnets can be beneficial, regardless of the goal; however, too much tapering is likely to lead to a degradation in other performance aspects of the machine.

The Δx values of Table III show how small the variations in the teeth/PM tips can be, suggesting that it is just as likely that the specific combination of tapering ratios, instead of one in particular, reduces the force ripple and cogging forces. This emphasises the importance of finding a robust design solution.

Some general guidelines can be given for the taper ratios. Keeping k_{c_N} between 0.65 and 0.7, k_{c_S} close to 0.7, k_m between 0.88 and 0.92 and k_t 0.6 is likely to produce the best results.

REFERENCES

[1] N. Baloch, S. Khaliq, and B.-I. Kwon, "A high force density HTS tubular vernier machine," *IEEE Transactions on Magnetics*, vol. 53, no. 11, pp. 1–5, 2017.

[2] A. A. Almoraya, N. Baker, K. Smith, and M. Raihan, "A new configuration of a consequent pole linear vernier hybrid machine with V-shape magnets," in *2018 XIII International Conference on Electrical Machines (ICEM)*. IEEE, 2018, pp. 2002–2008.

[3] Y. Gao, R. Qu, D. Li, and F. Chen, "Force ripple minimization of a linear vernier permanent magnet machine for direct-drive servo applications," *IEEE Transactions on Magnetics*, vol. 53, no. 6, pp. 1–5, 2017.

[4] C. Shi, R. Qu, D. Li, Y. Gao, and R. Li, "Comparative study on a novel consequent-pole modular linear vernier machine with PMs on both mover and stator iron cores," in *2019 IEEE Energy Conversion Congress and Exposition (ECCE)*. IEEE, pp. 712–716.

[5] A. Almoraya, N. Baker, K. Smith, and M. Raihan, "Development of a double-sided consequent pole linear vernier hybrid permanent-magnet machine for wave energy converters," in *2017 IEEE International Electric Machines and Drives Conference (IEMDC)*. IEEE, 2017, pp. 1–7.

[6] S.-U. Chung, H.-J. Lee, B.-C. Woo, J.-W. Kim, J.-Y. Lee, S.-R. Moon, and S.-M. Hwang, "A feasibility study on a new doubly salient permanent magnet linear synchronous machine," *IEEE Transactions on Magnetics*, vol. 46, no. 6, pp. 1572–1575, 2010.

[7] R. K. Roy, *Design of experiments using the Taguchi approach*. John Wiley & Sons, 2001.

[8] A. J. Sorgdrager, R.-J. Wang, and A. J. Grobler, "Multiobjective design of a line-start PM motor using the Taguchi method," *IEEE Transactions on Industry Applications*, vol. 54, no. 5, pp. 4167–4176, 2018.

[9] A. J. Sorgdrager, R.-J. Wang, and A. Grobler, "Taguchi method in electrical machine design," *SAIEE Africa Research Journal*, vol. 108, no. 4, pp. 150–164, 2017.

[10] M. S. Phadke, *Quality engineering using robust design*. Prentice Hall PTR, 1995.

[11] A. J. Sorgdrager, R.-J. Wang, and A. J. Grobler, "Retrofit design of a line-start PMSM using the Taguchi method," in *2015 IEEE International Electric Machines & Drives Conference (IEMDC)*. IEEE, 2015, pp. 489–495.

[12] J. Du, P. Lu, and D. Liang, "Optimal design of a linear transverse-flux machine with mutually coupled windings for force ripple reduction," *IET Electric Power Applications*, vol. 12, no. 2, pp. 271–280, 2017.

[13] J. Song, F. Dong, J. Zhao, S. Lu, S. Dou, and H. Wang, "Optimal design of permanent magnet linear synchronous motors based on Taguchi method," *IET Electric Power Applications*, vol. 11, no. 1, pp. 41–48, 2017.

VI. BIOGRAPHIES

Christoff D. Botha received the B.Eng and M.Eng degrees in Electrical and Electronic Engineering from Stellenbosch University South Africa, in 2015 and 2018, respectively. He is currently working towards the completion of a Ph.D. degree in the Department of Electrical and Electronic Engineering at Stellenbosch University. His current research focus is on linear electric machines and energy storage for use in renewable energy grid integration.

Maarten J. Kamper (SM'08) received the M.Sc. (Eng) and Ph.D. (Eng) degrees from the Stellenbosch University South Africa, in 1987 and 1996, respectively. In 1989, he joined the academic staff of the Department of Electrical and Electronic Engineering, Stellenbosch University, where he is currently a Professor of electrical machines and drives. His research area is computer-aided design and the control of reluctance, permanent magnet and induction electrical machine drives, with applications in electric transportation and renewable energy. Prof. Kamper is a South African National Research Foundation-supported scientist and a registered Professional Engineer in South Africa.

Rong-Jie Wang (SM'08) received the M.Sc. degree in electrical engineering from the University of Cape Town in 1998 and the Ph.D. degree in electrical engineering from Stellenbosch University in 2003, all in South Africa. He is currently an Associate Professor in the Department of Electrical and Electronic Engineering, Stellenbosch University. His research interests include novel topologies of permanent magnet machines, computer-aided design and optimisation of electrical machines, cooling design and analysis, and renewable energy systems.

Albert J. Sorgdrager (M13) received the B.Eng and M.Eng degrees in electrical engineering from North-West University, Potchefstroom, South Africa in 2010 and 2013, respectively, and the Ph.D. degree in electrical engineering from Stellenbosch University, South Africa in 2017. He is currently with Magna Powertrain, St. Valentin, Austria. His research interests include design framework development for traction drive applications, robust and traditional design optimisation methods and industrial drive systems.